

An Efficient Single-Input Multiple Output Power supply using DC–DC Boost Converter

P.Sridhar, P.Arulkumar

M.E(PED), King college of Technology, Nallur, Namakkal, Tamilnadu, India

ASP, Dept. of EEE, King college of Technology, Nallur, Namakkal, Tamilnadu, India

ABSTRACT: The aim of this study is to develop an high-efficient single-input multiple-output dc–dc boost converter. The proposed converter can boost the voltage of a low-voltage input power source to a controllable high-voltage dc bus and middle-voltage output terminals. The high-voltage dc bus can take as the main power for a high-voltage dc load or the front terminal of a dc–ac inverter. Moreover, middle-voltage output terminals can supply powers for individual middle-voltage dc loads or for charging auxiliary power sources (e.g., battery modules). In this study, a coupled-inductor based dc–dc converter scheme utilizes only one power switch with the properties of voltage clamping and soft switching, and the corresponding device specifications are adequately designed. As a result, the objectives of an high-efficient power conversion, high step up ratio, and various output voltages with different levels can be obtained. Some experimental results via a kilowatt-level prototype are given to verify the effectiveness of the proposed an efficient SIMO dc–dc boost converter in practical applications. In this dc dc converter we verified in simulation output wave form using matlab software.

Copyright to IJIRSET

I. INTRODUCTION

In order to protect the natural environment on the earth, the development of clean energy without pollution has the major representative role in the last decade [1]–[3]. By dealing with the issue of global warming, clean energies, such as fuel cell (FC), photovoltaic, and wind energy, etc., have been rapidly promoted. Due to the electric characteristics of clean energy, the generated power is critically affected by the climate or has slow transient responses, and the output voltage is easily influenced by load variations [4]–[6]. Besides, other auxiliary components, e.g., storage elements, control boards, etc., are usually required to ensure the proper operation of clean energy. For example, an FC-generation system is one of the most efficient and effective solutions to the environmental pollution problem [7]. In addition to the FC stack itself, some other auxiliary components, such as the balance of plant (BOP) including an electronic control board, an air compressor, and a cooling fan, are required for the normal work of an FC generation system [8], [9]. In other words, the generated power of the FC stack also should satisfy the power demand for the BOP. Thus, various voltage levels should be required in the power converter of an FC generation system. In general, various single-input single-output dc–dc converters with different voltage gains are combined to satisfy

the requirement of various voltage levels, so that its system control is more complicated and the corresponding cost is more expensive. The motivation of this study is to design a single-input multiple-output dc dc boost converter for increasing the conversion efficiency and voltage gain, reducing the control complexity, and saving the manufacturing cost.

Patra *et al.* [10] presented a SIMO dc–dc converter capable of generating buck, boost, and inverted outputs simultaneously. However, over three switches for one output were required. This scheme is only suitable for the low output voltage and power application, and its power conversion is degenerated due to the operation of hard switching. Namiet *al.* [11] proposed a new dc–dc multi-output boost converter, which can share its total output between different series of output voltages for low- and high-power applications. Unfortunately, over two switches for one output were required, and its control scheme was complicated. Besides, the corresponding output power cannot supply for individual loads independently. Chen *et al.* [12] investigated a multiple-output dc–dc boost converter with shared zero-current switching (ZCS) lagging leg. Although this converter with the soft-switching property can reduce the switching losses, this combination scheme with three full-bridge converters is more complicated, so that the objective of high-efficiency power conversion is difficult to achieve, and its cost is inevitably increased.

This study presents a newly designed SIMO converter with a coupled inductor. The proposed converter uses one power switch to achieve the objectives of high-efficiency power conversion, high step-up ratio, and different output voltage levels. In the proposed SIMO converter, the techniques of soft switching and voltage clamping are adopted to reduce the switching and conduction losses via the utilization of a low-voltage-rated power switch with a small $R_{DS(on)}$. Because the

slew rate of the current change in the coupled inductor can be restricted by the leakage inductor, the current transition time enables the power switch to turn ON with the ZCS property easily, and the effect of the leakage inductor can alleviate the losses caused by the reverse-recovery current. Additionally, the problems of the stray inductance energy and reverse-recovery currents within diodes in the conventional boost converter also can be solved, so that the high-efficiency power conversion can be achieved. The voltages of middle-voltage output terminals can be appropriately adjusted by the design of auxiliary inductors; the output voltage of the high-voltage dc bus can be stably controlled by a simple proportional-integral (PI) control.

II. CONVERTER DESIGN AND ANALYSES

The system configuration of the proposed high-efficiency SIMO converter topology to generate two different voltage levels from a single-input power source. This SIMO converter contains five parts including a low-voltage-side circuit (LVSC), a clamped circuit, a middle-voltage circuit, an auxiliary circuit, and a high-voltage-side circuit (HVSC). The major symbol representations are summarized as follows. V_{FC} (i_{FC}) and V_{O1} (i_{O1}) denote the voltages (currents) of the input power source and the output load at the LVSC and the auxiliary circuit, respectively; V_{O2} and i_{O2} are the output voltage and current in the HVSC. C_{FC} , C_{O1} , and C_{O2} are the filter capacitors at the LVSC, the auxiliary circuit, and the HVSC, respectively; C_1 and C_2 are the clamped and middle-voltage capacitors in the clamped and middle-voltage circuits, respectively.

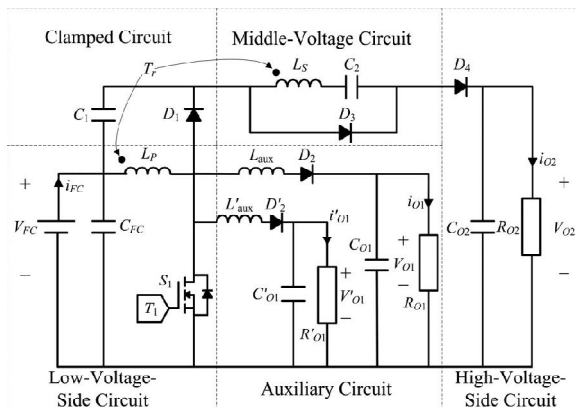


Fig. 1 System configuration of an high-efficient single-input multiple-output DC DC converter

L_P and L_S represent individual inductors in the primary and secondary sides of the coupled inductor Tr , respectively, where the primary side is connected to the input power source; L_{aux} is the auxiliary circuit inductor. The main switch is expressed as S_1 in the LVSC; the equivalent load in the auxiliary circuit is represented as RO_1 , and the output load is represented as RO_2 in the HVSC. The corresponding equivalent circuit is used to define the voltage polarities and current directions. The coupled inductor can be modeled as an ideal transformer including the magnetizing inductor L_{mp} and the leakage inductor L_{kp} . The turns ratio N and coupling coefficient k of this ideal transformer are defined as

$$N = N_2/N_1 \quad (1)$$

$$k = L_{mp}/(L_{kp} + L_{mp})$$

$$= L_{mp}/L_P \quad (2)$$

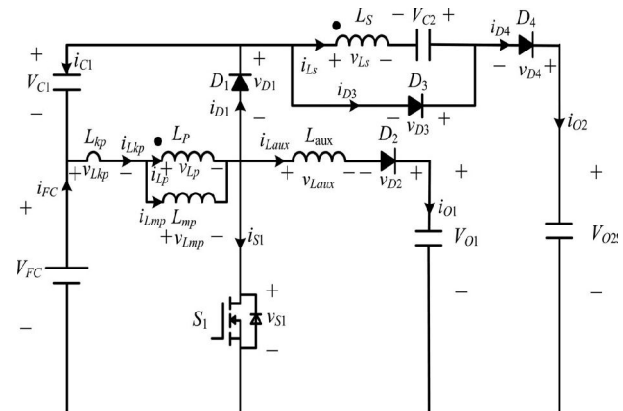


Fig. 2. Equivalent circuit.

where N_1 and N_2 are the winding turns in the primary and secondary sides of the coupled inductor Tr . Because the voltage gain is less sensitive to the coupling coefficient and the clamped capacitor C_1 is appropriately selected to completely absorb the leakage inductor energy [13], the coupling coefficient could be simply set at one ($k = 1$) to obtain $L_{mp} = L_P$ via (2). In this study, the following assumptions are made to simplify the converter analyses: 1) The main switch including its body diode is assumed to be an ideal switching element; and 2) The conduction voltage drops of the switch and diodes are neglected.

III. MODES OF OPERATION

1) *Mode 1* ($t_0 - t_1$) [Fig. 3(a)]: In this mode, the main switch S_1 was turned ON for a span, and the diode D_4 turned OFF. Because the polarity of the windings of the coupled inductor Tr is positive, the diode D_3 turns ON. The secondary current i_{Ls} reverses and charges to the middle voltage capacitor C_2 . When the auxiliary inductor L_{aux} releases its stored energy completely, and the diode D_2 turns OFF, this mode ends.

2) *Mode 2* ($t_1 - t_2$) [Fig. 3(b)]: At time $t = t_1$, the main switch S_1 is persistently turned ON. Because

the primary inductor LP is charged by the input power source, the magnetizing current $iLmp$ increases gradually in an approximately linear way. At the same time, the secondary voltage vLs charges the middle-voltage capacitor $C2$ through the diode

$D3$. Although the voltage $vLmp$ is equal to the input voltage VFC both at modes 1 and 2, the ascendant slope of the leakage current of the coupled inductor ($diLkp/dt$) at modes 1 and 2 is different due to the path of the auxiliary circuit. Because the auxiliary inductor $Laux$ releases its stored energy completely, and the diode $D2$ turns OFF at the end of mode 1, it results in the reduction of $diLkp/dt$ at mode 2.

3) *Mode 3 ($t2 - t3$)* [Fig. 3(c)]: At time $t = t2$, the main switch $S1$ is turned OFF. When the leakage energy still released from the secondary side of the coupled inductor, the diode $D3$ persistently conducts and releases the leakage energy to the middle-voltage capacitor $C2$. When the voltage across the main switch $vS1$ is higher than the voltage across the clamped capacitor $VC1$, the

diode $D1$ conducts to transmit the energy of the primary-side leakage inductor Lkp into the clamped capacitor $C1$. At the same time, partial energy of the primary-side leakage inductor Lkp is transmitted to the auxiliary inductor $Laux$, and the diode $D2$ conducts. Thus, the current $iLaux$ passes through the diode $D2$ to supply the power for the output load in the auxiliary circuit. When the secondary side of the coupled inductor releases its leakage energy completely, and the diode $D3$ turns OFF, this mode ends.

4) *Mode 4 ($t3 - t4$)* [Fig. 3(d)]: At time $t = t3$, the main switch $S1$ is persistently turned OFF. When the leakage energy has released from the primary side of the coupled inductor, the secondary current iLS is induced in reverse from the energy of the magnetizing inductor Lmp through the ideal transformer, and flows through the diode $D4$ to the HVSC. At the same time, partial energy of the primary side leakage inductor Lkp is still persistently transmitted to the auxiliary inductor $Laux$, and the diode $D2$

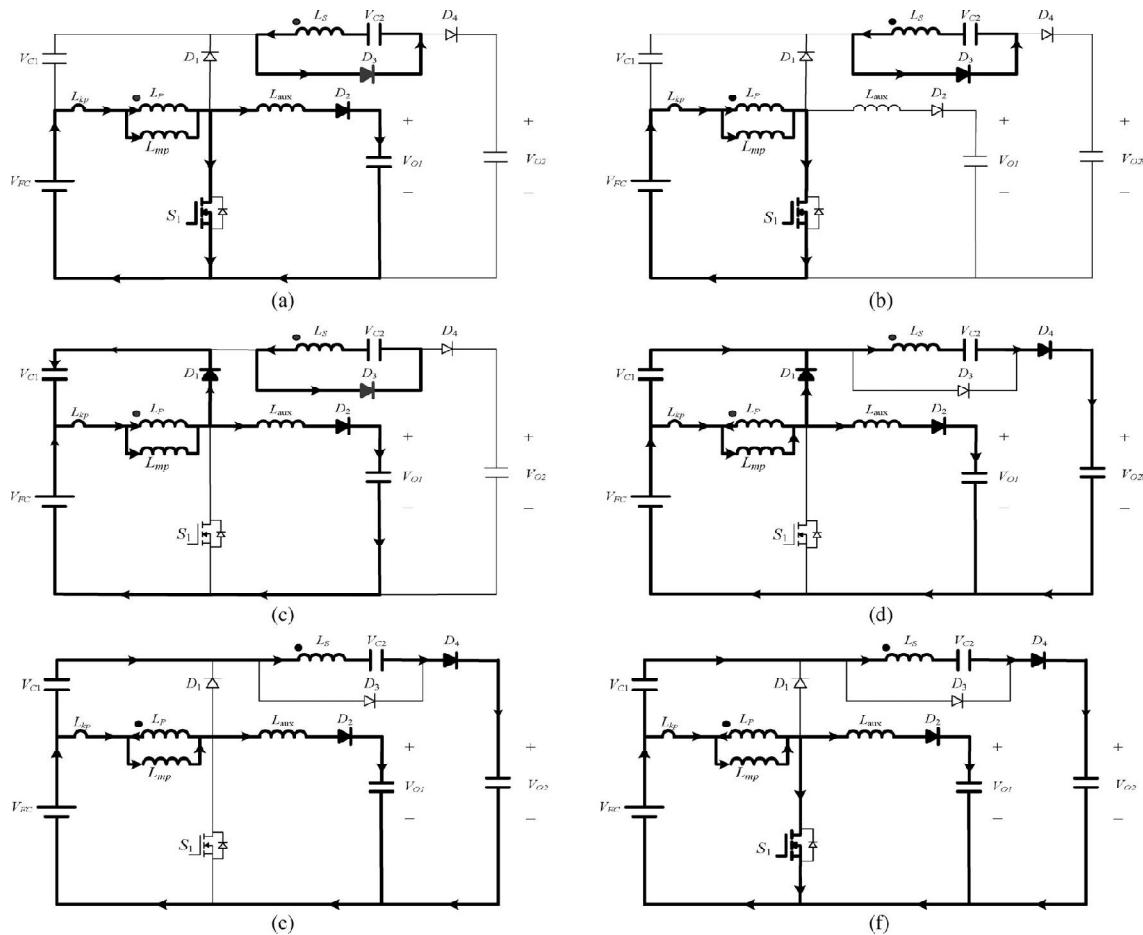


Fig. 3. Topological modes: (a) Mode 1 [t_0-t_1]; (b) Mode 2 [t_1-t_2]; (c) Mode 3 [t_2-t_3]; (d) Mode 4 [t_3-t_4]; (e) Mode 5 [t_4-t_5]; (f) Mode 6 [t_5-t_6].

keeps to conduct. Moreover, the current iL aux passes through the diode D_2 to supply the power for the output load in the auxiliary circuit.

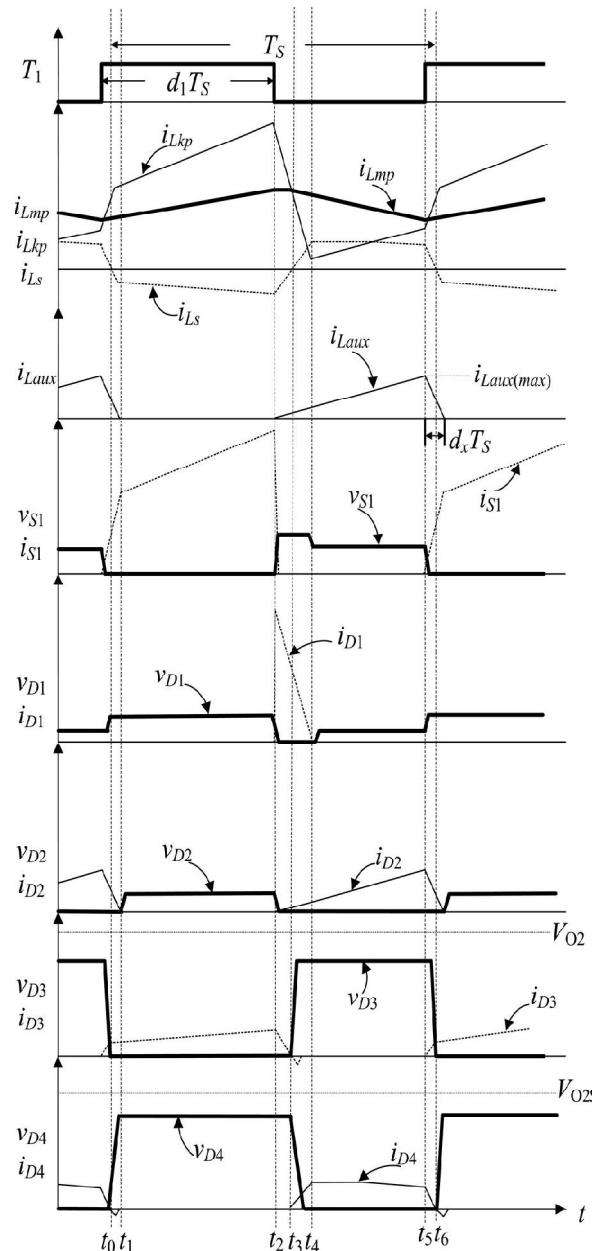
5) Mode 5 (t_4-t_5) [Fig. 3(e)]: At time $t = t_4$, the main switch S_1 is persistently turned OFF, and the clamped diode D_1 turns OFF because the primary leakage current $iLkp$ equals to the auxiliary inductor

current iL aux. In this mode, the input power source, the primary winding of the coupled inductor Tr , and the auxiliary inductor $Laux$ connect in series to supply the power for the output load in the auxiliary circuit through the diode D_2 . At the same time, the input power source, the secondary winding of the coupled inductor Tr , the clamped

capacitor $C1$, and the middle voltage capacitor ($C2$) connect in series to release the energy into the HVSC through the diode $D4$.

6) *Mode 6 ($t5 - t6$) [Fig. 3(f)]*: At time $t=t5$, this mode begins when the main switch $S1$ is triggered. The auxiliary inductor current iL_{aux} needs time to decay to zero, the diode $D2$ persistently conducts. In this mode, the input power source, the clamped capacitor $C1$, the secondary winding of the coupled inductor Tr , and the middle-voltage capacitor $C2$ still connect in series to release the energy into the HVSC through the diode $D4$. Since the clamped diode $D1$ can be selected as a low-voltage Schottky diode, it will be cut off promptly without a reverse-recovery current. Moreover, the rising rate of the primary current iL_{kp} is limited by the primary-side leakage inductor Lkp

Fig:4 Characteristic wave form of SIMO



International Journal of Innovative Research in Science, Engineering and Technology

An ISO 3297: 2007 Certified Organization,

Volume 3, Special Issue 1, February 2014

International Conference on Engineering Technology and Science-(ICETS'14)

On 10th & 11th February Organized by

Department of CIVIL, CSE, ECE, EEE, MECHANICAL Engg. and S&H of Muthayammal College of Engineering, Rasipuram, Tamilnadu, India

Thus, one cannot derive any currents from the paths of the HVSC, the middle-voltage circuit, the auxiliary circuit, and the clamped circuit. As a result, the main switch $S1$ is turned ON under the condition of ZCS and this soft-switching property is helpful for alleviating the switching loss. When the secondary current i_{LS} decays to zero, this mode ends. After that, it begins the next switching cycle and repeats the operation in mode 1.

IV MATLAB SIMULATION

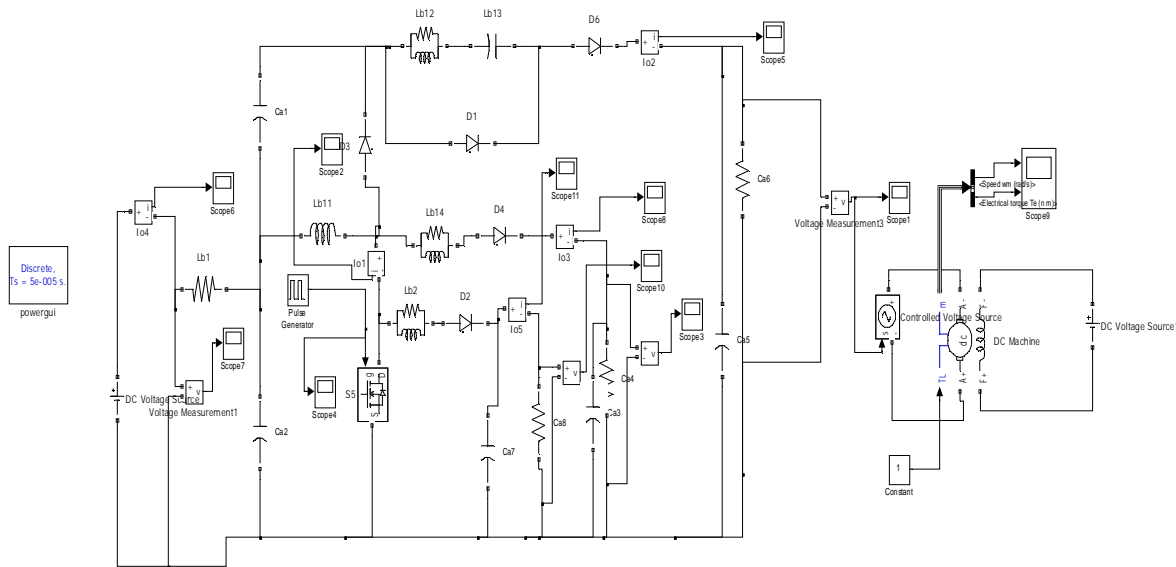
IN This project we are doing in matlab simulation software. here we discuss about in simulation block diagram, and output wave form for 200volt, 105volt and 24volt finally speed torque for separately excited dc motor. this dc motor is used for only output load verification.

V. CONCLUSION

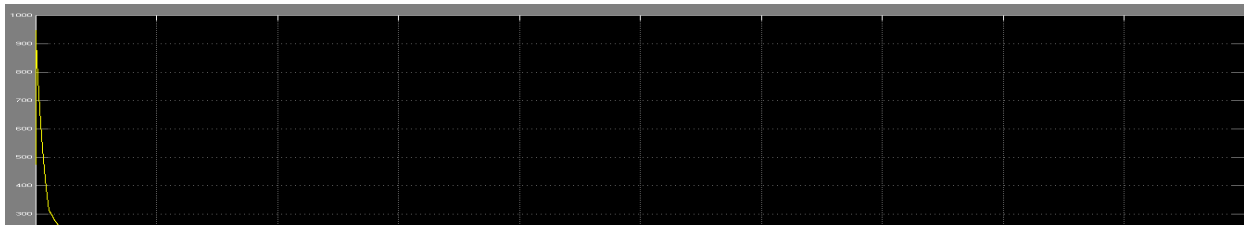
This study has successfully developed a high-efficiency SIMO dc-dc converter, and this coupled-inductor-based converter was applied well to a single-input power source plus two output terminals composed of an auxiliary battery module and a high-voltage dc bus. The experimental results reveal that the maximum efficiency was measured to exceed 95%, and the average conversion efficiency was measured over 91%. The proposed SIMO converter is suitable for the application required one common ground, which is preferred in

most applications. However, it is not appropriate to be used as the active front for dc-ac multilevel inverters. This limitation is worthy to be investigated in the future research. The major scientific contributions of the proposed SIMO converter are recited as follows: 1) this topology adopts only one power switch to achieve the objective of high-efficiency SIMO power conversion; 2) the voltage gain can be substantially increased by using a coupled inductor; 3) the stray energy can be recycled by a clamped capacitor into the auxiliary battery module or high-voltage dc bus to ensure the property of voltage clamping; 4) an auxiliary inductor is designed for providing the charge power to the auxiliary battery module and assisting the switch turned ON under the condition of ZCS; 5) the switch voltage stress is not related to the input voltage so that it is more suitable for a dc power conversion mechanism with different input voltage levels

VI. SIMULATION RESULT SIMULATION DIAGRAM



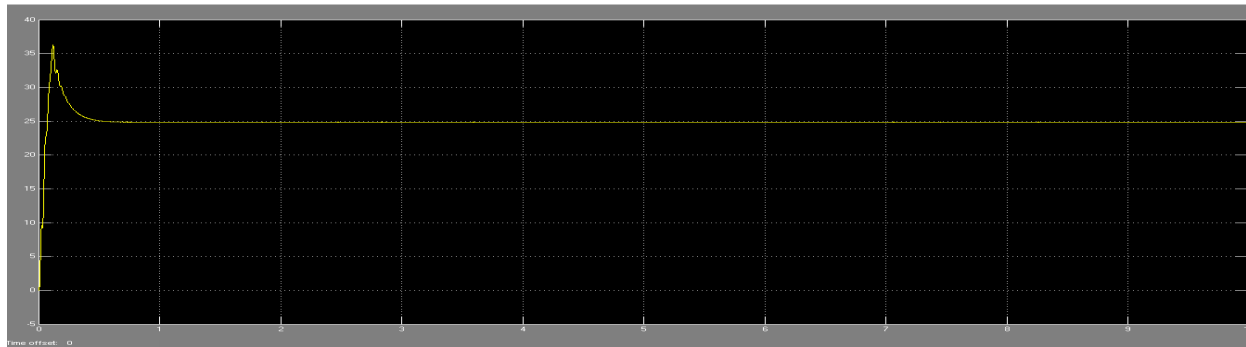
Output waveform For 200 volt



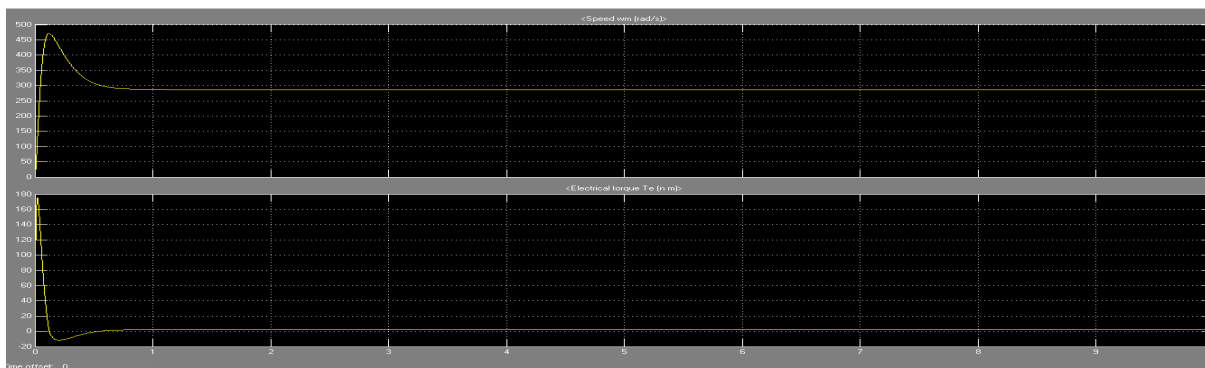
Output wave form For 105 volt



Output wave Form For 24 volt



Speed Torque Curve For Separately excited DC motor



and 6) the copper loss in the magnetic core can be greatly reduced as a full copper film with lower turns. high-efficiency SIMO converter topology provides designers with an alternative choice for boosting a low-voltage power source to multiple outputs with different voltage levels efficiently.

REFERENCES

- [1] A. Kirubakaran, S. Jain, and R. K. Nema, "DSP-controlled power electronic interface for fuel-cell-based distributed generation," *IEEE Trans. Power Electron.*, vol. 26, no. 12, pp. 3853–3864, Dec. 2011.
- [2] B. Liu, S. Duan, and T. Cai, "Photovoltaic dc-building-module-based BIPV system-concept and design considerations," *IEEE Trans. Power Electron.*, vol. 26, no. 5, pp. 1418–1429, May 2011.
- [3] M. Singh and A. Chandra, "Application of adaptive network-based fuzzy interference system for sensorless control of PMSG-based wind turbine with nonlinear-load-compensation capabilities," *IEEE Trans. Power Electron.*, vol. 26, no. 1, pp. 165–175, Jan. 2011.
- [4] C. T. Pan, M. C. Cheng, and C.M. Lai, "A novel integrated dc/ac converter with high voltage gain capability for distributed energy resource systems," *IEEE Trans. Power Electron.*, vol. 27, no. 5, pp. 2385–2395, May 2012.
- [5] S. D. Gamini Jayasinghe, D. Mahinda Vilathgamuwa, and U. K. Madawala, "Diode-clamped three-level inverter-based battery/supercapacitor direct integration scheme for renewable energy systems," *IEEE Trans. Power Electron.*, vol. 26, no. 6, pp. 3720–3729, Dec. 2011.
- [6] H. Wu, R. Chen, J. Zhang, Y. Xing, H. Hu, and H. Ge, "A family of threeport half-bridge converters for a stand-alone renewable power

International Journal of Innovative Research in Science, Engineering and Technology

An ISO 3297: 2007 Certified Organization,

Volume 3, Special Issue 1, February 2014

International Conference on Engineering Technology and Science-(ICETS'14)

On 10th & 11th February Organized by

Department of CIVIL, CSE, ECE, EEE, MECHANICAL Engg. and S&H of Muthayammal College of Engineering, Rasipuram, Tamilnadu, India

system,"*IEEE Trans. Power Electron.*, vol. 26, no. 9, pp. 2697–2706, Sep. 2012.

[7] M. W. Ellis, M. R. Von Spakovsky, and D. J. Nelson, "Fuel cell systems: Efficient, flexible energy conversion for the 21st century," *Proc. IEEE*, vol. 89, no. 12, pp. 1808–1818, Dec. 2001.

[8] T. Kim, O. Vodyakho, and J. Yang, "Fuel cell hybrid electronic scooter," *IEEE Ind. Appl. Mag.*, vol. 17, no. 2, pp. 25–31, Mar./Apr. 2011.

[9] F. Gao, B. Blunier, M. G. Simões, and A. Miraoui, "PEM fuel cell stack modeling for real-time emulation in hardware-in-the-loop application," *IEEE Trans. Energy Convers.*, vol. 26, no. 1, pp. 184–194, Mar. 2011.

[10] P. Patra, A. Patra, and N. Misra, "A single-inductor multiple-output switcher with simultaneous buck, boost and inverted outputs," *IEEE Trans. Power Electron.*, vol. 27, no. 4, pp. 1936–1951, Apr. 2012.

[11] A. Nami, F. Zare, A. Ghosh, and F. Blaabjerg, "Multiple-output DC–DC converters based on diode-clamped converters configuration: Topology and control strategy," *IET Power Electron.*, vol. 3, no. 2, pp. 197–208, 2010.

[12] Y. Chen, Y. Kang, S. Nie, and X. Pei, "The multiple-output DC–DC converter with shared ZCS lagging leg," *IEEE Trans. Power Electron.*, vol. 26, no. 8, pp. 2278–2294, Aug. 2011.

[13] R. J. Wai and R. Y. Duan, "High step-up converter with coupled inductor," *IEEE Trans. Power Electron.*, vol. 20, no. 5, pp. 1025–1035, Sep. 2005.

[14] N. Mohan, T. M. Undeland, and W. P. Robbins, *Power Electronics: Converters, Applications, and Design*. New York: Wiley, 1995.

[15] L. Schuch, C. Rech, H. L. Hey, H. A. Gründling, H. Pinheiro, and J. R. Pinheiro, "Analysis and design of a new high-efficiency bidirectional integrated ZVT PWM converter for DC-bus and battery-bank interface," *IEEE Trans. Ind. Appl.*, vol. 42, no. 5, pp. 1321–1332, Sep./Oct. 2006.

[16] Y. Chen and Y. Kang, "A full regulated dual-output dc-dc converter with special-connected two transformers (SCTTs) cell and complementary pulsewidth modulation-PFM (CPWM-PFM)," *IEEE Trans. Power Electron.*, vol. 25, no. 5, pp. 1296–1309, May 2010.

[17] J. K. Kim, S. W. Choi, and G. W. Moon, "Zero-voltage switching postregulation

scheme for multioutput forward converter with synchronous switches," *IEEE Trans. Ind. Electron.*, vol. 58, no. 6, pp. 2378–2386, [18] L. Hang, S. Wang, Y. Gu, W. Yao, and Z. Lu, "High cross-regulation multioutput LLC series resonant converter with Magamp postregulator," *IEEE Trans. Ind. Electron.*, vol. 58, no. 9, pp. 3905–3913, Sep. 2011.

[19] S. H. Cho, C. S. Kim, and S. K. Han, "High-efficiency and low-cost tightly regulated dual-output LLC resonant converter," *IEEE Trans. Ind. Electron.*, vol. 59, no. 7, pp. 2982–2991, Jul. 2012.